Kinetic aspects of resistive wall modes *

M. Mulec[1], I. B. Ivanov[1,2], M. F. Heyn[1], W. Kernbichler[1]

[1]*Association EURATOM-ÖAW, Institut für Theoretische Physik - Computational Physics,*

TU Graz, Austria

[2]*Petersburg Nuclear Physics Institute, Russia*

Introduction

In recent studies of the interaction of low frequency resonant magnetic field perturbations it has been demonstrated that MHD theory has strong limitations in its applicability for modern Tokamak parameter range [1]. Namely, the radial scale of resonant layers in plasma is comparable to the ion Larmor radius. Therefore, it is interesting to compare MHD results for various instabilities connected with resonant magnetic flux surfaces (kink modes, resistive wall modes) with results using the kinetic approach.

Code KiLCA (Kinetic Linear Cylindrical Approximation) is a wave code based on the kinetic description of the tokamak plasma in a periodic cylinder geometry [2,3]. The code has been successfully used to study kinetic effects of the interaction of resonant magnetic perturbations and the plasma in particular near resonant magnetic surfaces. The present report describes the modification of this code in such a way that also global modes and wave instabilities can be studied. The code is used to study kinetic effects including Landau damping and a proper account of particle collisions on the resistive wall mode. This is of particular interest if resonant magnetic surfaces are present in the plasma.

MHD modelling

In the present studies, results from ideal MHD modelling are compared to results from kinetic modelling. An ideal MHD equilibrium

$$\nabla p = \frac{1}{c}\,\mathbf{j_0}\times\mathbf{B_0}, \qquad \nabla\times\mathbf{B_0} = \frac{4\pi}{c}\mathbf{j_0},$$

is taken in one dimensional screw pinch symmetry. The ideal MHD equation are linearized and written in the form of an eigenvalue problem [4,5] for the displacemntvector $\boldsymbol{\xi}$,

$$-\omega^2\rho_0\,\boldsymbol{\xi} = \mathbf{F}\left(\boldsymbol{\xi}\right)$$

*This work, supported by the European Communities under the contract of Association between EURATOM and the Austrian Academy of Sciences, was carried out within the framework of the European Fusion Development Agreement. The views and opinions expressed herein do not necessarily reflect those of the European Commission. Additional funding is provided by the Austrian Science Foundation, FWF, under contract number P19889-N16.

where

$$\begin{aligned}\mathbf{F}(\boldsymbol{\xi}) &= \nabla\left(\boldsymbol{\xi}\cdot\nabla p_0+\gamma p_0\left(\nabla\cdot\boldsymbol{\xi}\right)\right)+\frac{1}{4\pi}\left[\left(\nabla\times\mathbf{B}_0\right)\times\mathbf{B}_1+\left(\nabla\times\mathbf{B}_1\right)\times\mathbf{B}_0\right].\\ &+ \nabla\cdot\left[\rho_0\boldsymbol{\xi}\left(\mathbf{v}_0\cdot\nabla\right)\mathbf{v}_0-\rho_0\mathbf{v}_0\left(\mathbf{v}_0\cdot\nabla\right)\boldsymbol{\xi}\right]+2i\omega\rho_0\left(\mathbf{v}_0\cdot\nabla\right)\boldsymbol{\xi}.\end{aligned}$$

In screw pinch symmetry, a system of ordinary differential equations for ξ_r and p^* is obtained

$$\begin{aligned}\frac{AS}{r}\frac{\mathrm{d}}{\mathrm{d}r}\left(r\xi_r\right)&=C_{11}\left(r\xi_r\right)-C_{12}p^*, & AS\frac{\mathrm{d}}{\mathrm{d}r}p^*&=C_{21}\left(r\xi_r\right)-C_{22}p^*,\\ p^*&=-\gamma p_0\nabla\cdot\boldsymbol{\xi}-\boldsymbol{\xi}\cdot p_0+\frac{\mathbf{B}\cdot\mathbf{B_1}}{4\pi}, & \tilde{\omega}&=\omega-\frac{mv_\theta}{r}-kv_z,\\ A&=\rho_0\tilde{\omega}^2-\frac{F^2}{4\pi}, & S&=\left(\frac{B_\theta^2}{4\pi}+\gamma p_0\right)\rho_0\tilde{\omega}^2-\gamma p_0\frac{F^2}{4\pi},\\ C_{11}&=\rho_0\tilde{\omega}^2\frac{Q}{r}-2m\frac{ST}{r^3}, & C_{12}&=\rho_0^2\tilde{\omega}^4-\left(k^2+\frac{m^2}{r^2}\right)S,\\ C_{21}&=\frac{AS}{r}C_4-4\frac{ST^2}{r^3}+\frac{Q^2}{r^3}, & C_{22}&=rC_{11},\\ T&=\frac{FB_\theta}{4\pi}+\rho_0\tilde{\omega}v_\theta, & C_4&=A+r\frac{\mathrm{d}}{\mathrm{d}r}\left(\frac{B_\theta^2-4\pi\rho_0v_\theta^2}{4\pi r^2}\right),\end{aligned}$$

$$Q=\rho_0\tilde{\omega}^2\left(\frac{B_\theta^2}{4\pi}-\rho_0v_\theta^2\right)+\frac{\rho_0}{4\pi}\left(B_\theta\tilde{\omega}+Fv_\theta\right)^2.$$

Kinetic modelling

In the kinetic modelling we solve Vlasov equation

$$\frac{\partial f}{\partial t}+\nabla\cdot\left(f\mathbf{v}\right)+\frac{F}{m}\frac{\partial f}{\partial v}=\frac{\partial}{\partial v}D_{\alpha\beta}\frac{\partial f}{\partial v}\ , \tag{1}$$

in cylindrical geometry [2,3]. The Coulomb collision operator is modelled by a charge conserving Fokker-Planck operator [3]. The perturbation field is determined by Maxwell equations

$$\nabla\times\mathbf{E}=\frac{i\omega}{c}\ \mathbf{B}\quad,\quad\nabla\times\mathbf{B}=-\frac{i\omega}{c}\ \mathbf{E}+\frac{4\pi}{c}\ \mathbf{j}. \tag{2}$$

From the kinetic model we obtain the current density

$$\mathbf{j}=e\int\mathrm{d}^3p\ \mathbf{v}\ f\ , \tag{3}$$

which is used in Maxwell equations.

Numerical realization

Maxwell equations with electrical charge and current density obtained from either the fluid model or the kinetic model are solved for a straight periodic cylinder. Fourier transforming with respect to time as well as poloidal and toroidal angles yields a set of ordinary

differential equations for the different eigenmodes. The various modes have very different scales and an appropriate solver for the boundary value problem has to be used. Basic solutions in 5 different regions, namely two plasma regions, a vacuum region, a resistive wall region of finite size, and an outside vacuum region for arbitrary frequency ω are constructed. The vacuum as well as the resistive wall region solutions are obtained analytically. Finally ω is obtained such that the solutions can be matched appropriately at the freely chosen radius within the plasma region. From this the dispersion relation for the eigenfrequency ω of the modes follows.

Numerical profiles for the chosen equilibrium are shown in Fig. 1. This gives a characteristic time $\tau_A = R/V_A$ with big radius R and the Alfvén speed V_A for magnetic axis values of field and density. The chosen profile of the toroidal frequency in units of the Alfvén frequency is also shown in Fig. 1. The different regions and a sketch of the matching procedure is sketched in Fig. 2.

Results

For poloidal mode number $m = -1$ and toroidal mode number $n = 1$, the resonant surface is at $r/r_p \approx 0.8$. For this mode numbers, an unstable global mode has been found for the MHD model as well as for the kinetic model of the current density. The corresponding results for the Fourier components of the radial magnetic field perturbation (eigenfunctions) are shown in the left of Fig. 3 for zero toroidal plasma velocity. In ideal MHD, the Fourier component is purely real whereas in the kinetic model it is complex due to Landau damping and the account of collisions. The solutions are seen to be in qualitative agreement. The corresponding growth rates are shown on the right of Fig. 3 as a function of the toroidal rotation frequency and are about 10 % of the Alfvén frequency. The modes are stabilized for a certain value of the toroidal rotation frequency. The threshold value for the kinetic model is observed to be visibly smaller than the corresponding value for the MHD model. Such a behavior has also been observed in a previous study where some kinetic effects on the growths rates of resistive wall modes have been considered [6].

References

[1] M. F. Heyn, I. B. Ivanov, S. V. Kasilov, et al, Nucl. Fusion **48**, 024005 (2008).

[2] M. F. Heyn, I. B. Ivanov, S. V. Kasilov, et al, Nucl. Fusion **46**, S159 (2006).

[3] I. B. Ivanov, M. F. Heyn, S. V. Kasilov, et al, Phys. Plasmas **18**, 022501-1 (2011).

[4] J. P. Freidberg, Phys. Fluids **13**, 1812 (1970).

[5] A. Bondenson, R. Iacono, A. Bhattacharjee, Phys. Fluids **30**, 2167 (1987).

[6] Y. Liu, A. Bondenson, Y. Gribov, and A. Polevi, Nuclear fusion **44**, 232 (2004).

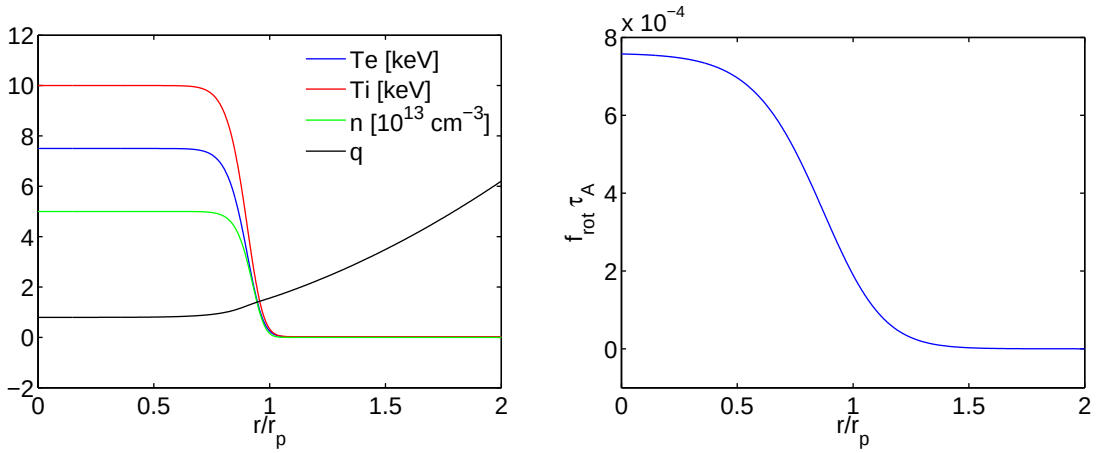

Fig. 1. Left: Profiles for density n, temperatures T_i, T_e, and safety factor q over normalized plasma radius r_p. Right: Profile for the toroidal rotation frequency.

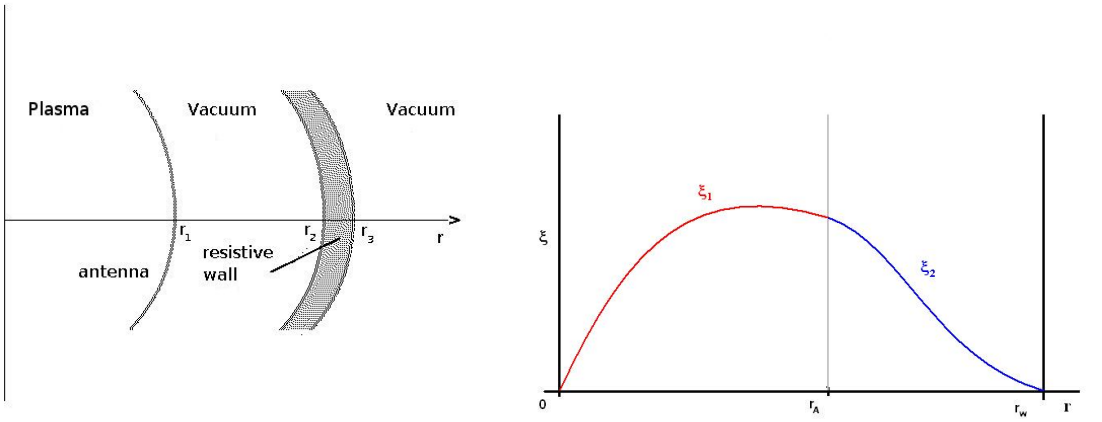

Fig. 2. Left: Different regions: plasma region, vacuum region, resistive wall region, and outside vacuum region. Right: Eigenfunctions are computed and the dispersion follows from the continuity conditions at some arbitrary radius.

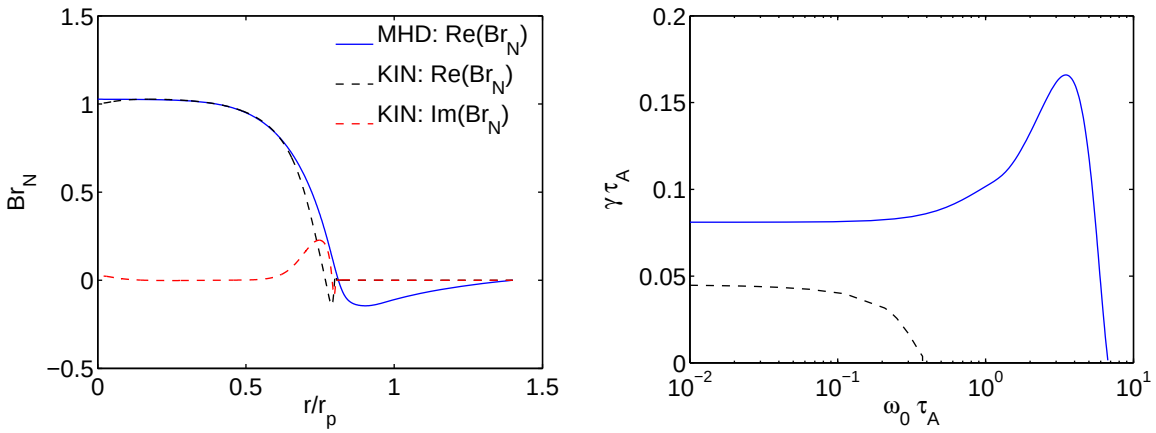

Fig. 3. Left: Comparison of the Fourier components of the radial magnetic field perturbation for the ideal MHD modelling and the kinetic modelling. Right: Growth rate γ normalized to the Alfén time τ_A as a function of the normalized toroidal rotation frequency (ω_0 is the rotation frequency at $r = 0$). Solid line is the ideal MHD result and dashed line is the kinetic modelling result.